Soft Matter

PAPER

View Article Online
View Journal

Cite this: DOI: 10.1039/d5sm01014d

Influence of block microstructure on the interaction of styrene-maleic acid copolymer aggregates and lipid nanodiscs

George M. Neville, [ab] Aya A. Nasser, [c] James Doutch, [d] Stephen King, [d] Pedro Estrela, [aef] Paul Whitley, [g] Gareth J. Price *[bc] and Karen J. Edler *[abh]

Investigation of the properties of membrane proteins (MPs) is essential to the successful development of medicines and biotechnology. However, their study is often complicated by denaturation caused by the use of detergents during conventional extraction methods. Copolymers of styrene and maleic acid (SMA) have shown promise in extracting MPs directly from cells while reconstituting lipid membranes into nanodiscs. Despite their potential, there remains a dearth of information on the precise interactions that take place between the copolymers and lipid membranes although they are known to be sensitive to small variations in copolymer composition or structure. We have used reversible addition–fragmentation chain transfer (RAFT) polymerisation to synthesise SMA copolymers with equivalent molar mass, but with inverted block sequences and end group termini. Through a range of experiments, including dynamic light scattering and small-angle neutron scattering (SANS) on SMA aggregates and nanodisc formation studies using UV-vis spectroscopy with both model DMPC lipids and *E. coli* membranes, the impact of both block distribution and end group chemistry on copolymer–membrane interactions was investigated. It was found that mismatched hydrophilic and hydrophobic end groups on the styrene block and alternating block, respectively, impeded membrane disruption and subsequent solubilisation. This highlights not only how the amphiphilic balance of these blocks is important for efficient nanodisc formation, but also how end groups influence these and may be optimised towards extraction of more challenging MPs. The work contributes to a better understanding of SMA behaviour and offers insight into how these nanomaterials may be better designed and tailored for specific applications.

Received 3rd October 2025,
Accepted 2nd January 2026

DOI: 10.1039/d5sm01014d

rsc.li/soft-matter-journal

Introduction

Cell membranes are vital to organisms in securing the contents of the cell and in controlling signalling and material exchange with the external environment. Membrane proteins (MPs), which carry out these functions, are therefore important pharmaceutical drug targets[1,2] and have many potential biotechnological applications.[3–5]

When extracting MPs from cells for study, detergents interrupt the weak stabilising interactions both within a protein, as well as with the surrounding lipid membrane.[4,6] This can result in the loss of the original structure and hence active form of the protein. While development of cryo-EM structure determination has reduced the requirement for crystal-based structure determination, the denaturation of MPs when using detergents for extraction remains an issue.[6] MPs persistently account for a disproportionately small fraction of the Protein Structural Data Bank.[7] There is a need to be able to extract MPs in an unaltered state, not only to facilitate structural studies, but also so that their properties may be exploited in therapeutic or sensing applications.[8,9] Several methods have arisen to better stabilise MPs *ex vivo* through the use of membrane mimetic systems, such as amphipols[10] and membrane scaffold proteins (MSPs).[11] Although these have been widely investigated, these methods still require the use of detergents during workup.[6]

[a] *Centre for Sustainable Chemical Technologies, University of Bath, Bath, BA2 7AY, UK*
[b] *Department of Chemistry, University of Bath, Claverton Down, Bath, BA2 7AY, UK. E-mail: g.j.price@bath.ac.uk*
[c] *Department of Chemistry, Khalifa University, P.O. Box 127788, Abu Dhabi, UAE*
[d] *ISIS Pulsed Neutron and Muon Source, STFC Rutherford Appleton Laboratory, Harwell Campus, Didcot, OX11 0QX, UK*
[e] *Centre for Bioengineering & Biomedical Technologies (CBio), University of Bath, Claverton Down, Bath, BA2 7AY, UK*
[f] *Department of Electrical Engineering, University of Bath, Claverton Down, Bath, BA2 7AY, UK*
[g] *Department of Life Sciences, University of Bath, Claverton Down, Bath, BA2 7AY, UK*
[h] *Centre for Analysis and Synthesis, Department of Chemistry, Lund University, PO Box 124, 22100 Lund, Sweden*

More recently, copolymers of styrene and maleic acid, SMA, have shown particular promise for their ability to extract MPs directly from cells and stabilise them without the use of detergents while also retaining the lipid environment from the natural cell membrane.[6,12] By intercalating hydrophobic styrene moieties within the lipid tail groups,[13–15] the membrane is disrupted[13,16–19] following which self-assembly takes place into a 'styrene maleic acid lipid particle' (SMALP), or 'nanodisc'.[15,20,21] These can be suspended in aqueous solution and have a structure shown schematically in Fig. 1.[15] Whilst a useful model, the schematic presented in Fig. 1 is highly idealised; in fact the copolymer annulus will likely have an irregular ring shape[21] and may extend into the nanodisc core,[22] as well as to some extent possibly wrap around the nanodisc faces.[20] While SMA provides several analytical benefits,[23] and can now be readily sourced commercially (*e.g.*, from Anatrace, CubeBiotech, or Orbiscope),[24] a much more complicated and dynamic picture of SMALP structure and behaviour has emerged. This includes ongoing lipid exchange between SMALPs and membranes[25–31] and structural effects arising from interaction with the copolymer, such as broadened lipid gel-transitions with increased temperature[15,32] and lateral ring-tension within the disc.[33]

It is now well appreciated that it is challenging to find any single metric that accurately summarises the formation and behaviour of SMALPs. For example, loss of turbidity, and hence lipid molecules from larger vesicles into smaller particles, does not always directly relate to efficient protein extraction.[34–37] Likewise, the extent of insertion of the copolymer into the membrane appears not to be the only rate determining step.[38] The importance of SMA-only particles present in aqueous suspensions of high ionic strength has also become apparent.[18,34,58] These aggregates must first dissociate prior to membrane disruption,[39] and hence their physiochemical properties could give mechanistic insights into their performance. Thus, it is helpful to combine data from a range of complementary methods and evaluate an overall picture of aggregate and nanodisc interactions.

In order to overcome some of the limitations of SMA, such as its narrow pH tolerance, sensitivity to divalent cations and the potential effect of spectroscopic screening by styrene, alternative amphiphilic copolymers have been synthesised,[40] including SMI,[30,41] SMA-EA,[42] AASTY[43] and DIBMA.[25,44] While these work over a wider range of experimental conditions, there remains a lack of detailed mechanistic information regarding the interactions of the copolymers in solution with lipids and cell membranes. The issue is further exacerbated by the widespread reliance on pseudo-random commercial SMA copolymers including SMA 2000 (Cray Valley), used as a comparator in this study, which are sometimes poorly characterised and highly heterogeneous. Synthesised by starved-feed free-radical polymerisation, these materials often have broad molar mass and/or composition distributions making it difficult to isolate any single effect arising directly from the copolymer microstructure. Along with varying laboratory practices during use[17,34,45] this makes comparison of disparate data difficult. Hence, better control in both the synthesis of copolymers and the evaluation of their performance, is needed.

Reversible addition–fragmentation chain transfer (RAFT) has been employed by Cunningham *et al.*,[38] Kopf *et al.*,[35] as well as others[26,30,40,41,46] as a means of achieving SMA copolymers with a low dispersity, consistent composition and well defined structure distribution. Maleic anhydride is used as the second monomer which is readily converted to the acid form post-polymerisation. Due to the relative reactivity ratios of these monomers, and closed nature of this type of polymerisation, typically the resulting copolymers have a block architecture consisting of a block of alternating Sty-MA attached to a styrene block (Fig. 2a) with a short statistical gradient between the two. The lengths of the two blocks are controlled by the relative amounts of the two monomers in the feed. As the SMA copolymers used for membrane solubilisation are typically of

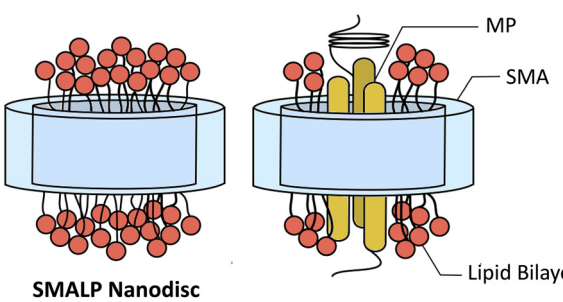

Fig. 1 Schematic of SMALP nanodisc structure with SMA copolymer annulus wrapped around a fragment of lipid bilayer able to encapsulate MPs. Variations of figures used in previous work.[22,39]

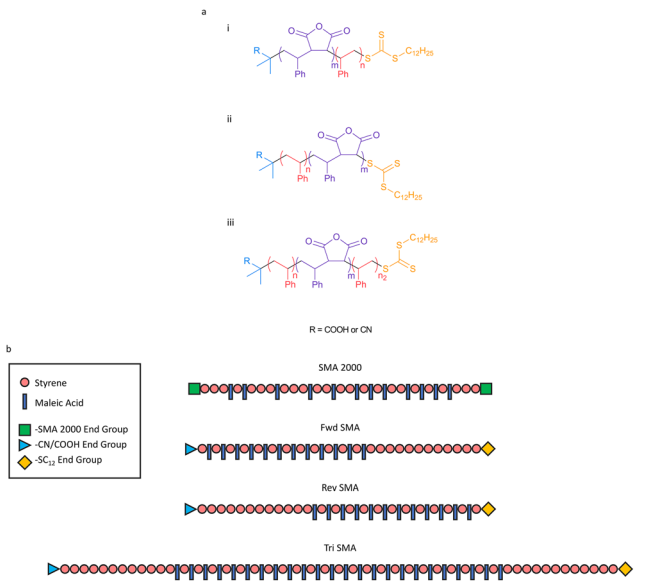

Fig. 2 (a) Chemical structure of copolymers from 2 : 1 RAFT copolymerisation (i) Forward styrene-maleic anhydride, denoted 'Fwd SMAnh' (ii) Reverse styrene-maleic anhydride, denoted 'Rev SMAnh' (iii) Triblock styrene-maleic anhydride, denoted 'Tri SMAnh'. (b) Schematic target chain structures of 2 : 1 pseudorandom and block SMA copolymer structures, after hydrolysis to the acid form.

low molar mass (<10 kDa), the gradients between these blocks can comprise at most two or three monomer units.

Another difference is that RAFT polymerisations result in chains with a hydrophobic end group, dependent on the RAFT-agent used. Typically this is 2-(dodecylthiocarbonothioylthio)-2-methylpropionic acid, DDMAT, which affords a relatively large SC_{12} unit (Fig. 2), which can account for ~10% by mass of commonly used SMA chains with a molar mass around 6 kDa. Our previous work showed the end group to significantly influence the copolymer behaviour.[22] For example, replacing the SC_{12} end group for a more polar CN group allowed RAFT-synthesised SMA to solubilise DPPC lipids. While RAFT-copolymers also tend to form larger nanodiscs, they appear to do so more slowly than the commercial variants and it seems that molar mass has less effect than the composition or amphiphilic balance.[38,46,47] The relative length of the styrene block also seems to play a role in driving membrane interactions.[48] If these effects could be better understood, it may be possible to exploit the properties of polymer end groups to expand upon the application of SMA. Moreover, these end groups also represent chemical functionality that could be exploited for property modification.

In this work, we have used RAFT reactions to produce copolymers with different arrangements of the end groups and the two monomers within the blocks. Schematics to demonstrate the various target structures are presented in Fig. 2b. Compared with previously produced copolymers, a 'reverse' structure inverts the end groups relative to the copolymer blocks. Assuming ideal polymerisation, this would result in SC_{12} groups on the hydrophilic alternating block, rather than the styrene block (Fig. 2a(ii)).[49] The hydrophobic styrene block would then be capped by a hydrophilic CN/COOH group. The RAFT technique also lends itself to the creation of 2 : 1 triblock materials and a polymer with two styrene blocks of equivalent length, one terminated by a SC_{12} and the other by a COOH/CN group, has been produced for further investigation (Fig. 2a(iii)).

For additional insight, RAFT copolymers were further compared with a commercial SMA 2000 variant (Cray Valley).[50] SMA 2000 has no block structure and the end groups are not expected to be very large or significantly affect polarity, being mostly cumyl groups.

The aim of this study was therefore to synthesise SMA copolymers with equivalent molar masses but inverted block sequences from RAFT copolymerisation in order to explore the effects of block microstructure on self-assembly in solution and in the presence of lipids. Resultant SMA aggregates, SMALP nanodiscs, as well as the transition between these nanostructures, were investigated to explore the interplay between copolymer end groups and block architecture, seeking to define its impact upon interaction with membranes.

Experimental

Materials

Before use, styrene (Sty) or d_8-styrene (dSty) (Merck, purity ≥99%) was passed through a pre-packed column (Merck) to remove the inhibiting agent, 4-*tert*-butylcatechol. The following were all purchased from Merck and used as received: The second monomer, maleic anhydride (MAnh) (purity ≥99%), the initiator, 2,2′-azobis(2-methylpropionitrile) (AIBN) (purity 98%), the RAFT agent, 2-(dodecylthiocarbonothioylthio)-2-methylpropionic acid (DDMAT) (purity 98%), the solvent, 1,4-dioxane (HPLC grade, purity >99.5%) and NaOH (anhydrous pellet, reagent grade, purity >98%) used for hydrolysis. The model lipid species, 1,2-dimystoyl-*sn-glycero*-3-phosphocholine (DMPC) (purity >99%) was also purchased from Merck and the deuterated version (d_{54}-DMPC) (purity >99%) purchased from Avanti Polar Lipids. The commercial SMA 2000 copolymer, which has a 2 : 1 styrene to maleic anhydride molar ratio was provided by Cray Valley. Mono and dibasic sodium phosphate (purity ≥99%) for buffer preparation were purchased from Acros Organics.

Synthesis of copolymers by reversible addition–fragmentation chain transfer polymerisation

The RAFT copolymer with the structure commonly synthesised by RAFT, coded 'Fwd SMAnh', was synthesised as described previously,[20,22,39,48] following the work of Harrison and Wooley[51] (Scheme S1 in SI). Here, the SC_{12} end group afforded by RAFT is generated on the styrene block. The molar ratios of the monomers, initiator and RAFT agent are given in Table S1 (SI).

Alternative arrangements of the copolymer components were produced *via* a two-step reaction (Scheme S2, SI) to produce chains with the end groups reversed, coded 'Rev SMAnh', or in a triblock configuration, coded 'Tri SMAnh', as shown in Fig. 2. In brief, the styrene block is grown first to produce what is effectively a polystyrene macro-RAFT agent onto which is grown the alternating styrene – maleic anhydride block. Experimental details are given in Tables S2 and S3 in the SI.

All SMAnh containing copolymers were hydrolysed to the acid form, SMA, by heating a 10% (w/v) aqueous polymer solution in 1 M NaOH under the previously reported conditions[20,22,39,48] (Scheme S3, SI).

Chromatographic and spectroscopic characterisation of copolymers

The molar masses of SMAnh copolymers and Sty macro-RAFT agents were estimated by GPC using an Agilent GPC 1260 Infinity chromatograph using two Pl gel 5 μm MIXED-D 30 cm × 7.5 mm columns with a guard column Pl gel 5 μm MIXED Guard 50 × 7.5 mm. The column oven was maintained at 35 °C, with GPC-grade THF as the eluent at a flow rate of 1.00 mL min^{-1} and refractive index detection using polymer concentrations between 1–2 mg ml^{-1}. The system was calibrated against 12 low dispersity polystyrene standards with a range of weight-averaged molar masses, M_w, from 1050 Da to 2650 kDa. Chromatograms were analysed with Agilent GPC/SEC software.

^{1}H NMR spectra were recorded using an Agilent 500 MHz NMR spectrometer from SMAnh polymer samples dissolved in d_6-acetone (40 mg mL^{-1}). Spectra were processed and analysed with Mestrelab Mnova 11.0 software. ^{13}C spectra were recorded with the same method but lengthened acquisition times to

improve signal-to-noise ratios. FTIR spectra were recorded on a PerkinElmer ATR desktop spectrometer with solid copolymer samples at room temperature using 16 scans with a resolution of 1 cm^{-1}. UV-vis spectra of aqueous suspensions of SMA in PBS were recorded using an Agilent Technologies Cary 60 UV-vis spectrometer and a quartz cuvette scanning in 1 nm intervals at 600 nm min^{-1}.

Preparation of phosphate buffer solution (PBS)

A 50 mM phosphate buffer solution (PBS) was made by mixing 0.1 M aqueous solutions of monobasic sodium phosphate (2.65 mL, 0.265 mmol) and dibasic sodium phosphate (47.35 mL, 4.735 mmol), and diluting to 100 mL with 18.2 MΩ cm ultra-filtered water. NaCl (1.1688 g, 20 mmol) was then added, resulting in a 0.2 M salt concentration. This produced a PBS stabilised at pH 8.0, confirmed using a Mettler Toledo S20 SevenEasy pH meter.

Dynamic light scattering (DLS)

DLS was conducted using a Malvern Zetasizer Nano Series, using either disposable plastic cuvettes for size measurements, or folded capillary zeta cells for zeta potential. Measurements were taken using a backscattering detector (θ = 173°) at a laser wavelength λ = 633 nm. All values reported relate to volume particle size distributions. In all cases, five sets of measurements were averaged, each consisting of at least 12 runs. Errors in diameter were reported as 95% confidence intervals calculated from the SD about the mean. The dispersity in this context was calculated as $(SD/mean)^2$, where a dispersity <0.1 was considered monodisperse.

Pendant drop tensiometry

Tensiometry was conducted on a FTA1000 contact angle/surface tension analyser and processed using FTA 32 surface tension image analysis software. Syringe needles were prepared by extensive washing with water, ethanol and acetone to remove contaminants. Samples containing SMA polymers in solution at 1.65 wt%. in PBS were then passed through these needles to produce a small hanging droplet that was typically imaged at a rate of 10 images per second for 10 s to ensure a good average measurement. The software was calibrated against 18.2 MΩ cm ultra-filtered water with an air–water surface tension of 72.15 mN m^{-1}. The magnification and distance between the camera and the drop was calibrated against the diameter of the needle (0.6419 mm).

Differential scanning calorimetry (DSC)

DSC was conducted on a TA Q20 Instrument with a ramp range between 70–400 °C using samples of known weight (1.5–2.0 mg) in crimped T_{zero} aluminium pans under purge of N_2 gas (18 mL min^{-1}) calibrated against an indium standard. Samples were equilibrated at 20 °C before being heated at a rate of 10.0 °C min^{-1} to 200 °C. This was held isothermally for 2 min before cooling at a rate of 10.0 °C min^{-1} to 20 °C and repeating the cycle.

E. coli membrane preparation

E. coli were grown in lysogeny broth (5 g tryptone, 5 g NaCl and 2.5 g yeast extract per litre) in a shaking incubator overnight at 37 °C. Cells were harvested by centrifugation at 5000× *g* for 10 min at 23 °C. 7.5 g of cell paste was resuspended in 30 mL PBS (50 mM phosphate, 200 mM NaCl, pH 8.0), 430 μL lysozyme (20 mg ml^{-1}), 30 μL $MgCl_2$ (1 M) and 30 μL DNase (20 mg ml^{-1}) prior to sonication for 5 min cumulatively (15 s on, 30 s off) on ice. The suspension was then centrifuged at 20 000× *g* for 10 min to remove unbroken cells and cell debris. The supernatant was collected and then centrifuged in an Optima Ultracentrifuge at 155 000× *g* using an MLA-80 rotor for 45 min. The pellet, which contained the membrane fraction, was collected and then resuspended in 5 ml PBS. Immediately prior to use, a short centrifugation at 1000× *g* for 1 min was used to remove any remaining cell debris, before the supernatant was further diluted with PBS to the desired concentration.

Nanodisc preparation

Nanodiscs were prepared in 50 mM (0.2 M NaCl) PBS stabilised at pH 8.0. The lipids (5.0 mg), DMPC or d_{54}-DMPC, were suspended in 680 μL PBS and sonicated in two 10 s bursts, with a 50% duty cycle, separated by a 15 s rest period to prevent overheating. 15 mg of copolymer in 230 μL PBS were then added, resulting in a nanodisc solution consisting of 1.65% (w/v) copolymer and 0.55% (w/v) lipid. An indication of successful nanodisc formation arises from the loss of turbidity upon the addition of copolymer.

Kinetics of nanodisc formation

Measurements were taken using an Agilent Technologies Cary 60 UV-vis spectrometer equipped with a Quantum Northwest TC 1 temperature controller. Quartz cuvettes with a 1 cm path length were loaded with 680 μL freshly sonicated lipid suspension (5 mg for DMPC; *E. coli* matched to 1.5 a.u. starting absorbance) in PBS with a stirrer bar and the temperature set. Separately, 15 mg SMA was dissolved in 230 μL PBS. The absorbances from the lipid suspensions were monitored before manual injection of the copolymer solution using an Eppendorf pipette at 130 s. The monitoring wavelength of 450 nm was chosen to avoid the absorbance from styrene (260 nm) or the SC_{12} RAFT end groups (310 nm), but still display enough variance related to turbidity in the visible range. Data were recorded at 0.0125 s intervals and smoothed using a nine-point moving average, equivalent to averaging each reading over 0.1 s. A separate experiment, where lipid suspensions were diluted with PBS without any copolymer, provided a reference to account for dilution effects.

Small angle neutron scattering (SANS)

SANS measurements were performed at the ISIS Neutron and Muon Source (Rutherford Appleton Laboratory, Didcot, UK) on the SANS2D beamline, with the two, two-dimensional, position-sensitive detectors situated 4 and 8 m behind the sample, respectively, and offset to either side of the transmitted beam.

In this instrument configuration, each detector overlaps in Q-space giving a simultaneously accessible Q-range of $\sim$0.003–0.9 Å^{-1} (equivalent d-spacings 7–2000 Å) using neutron wavelengths from $1.75 \leq \lambda \leq 12.5$ Å where $Q = (4\pi/\lambda)\sin\theta$ and 2θ is the scattering angle. The neutron beam was collimated to 8 mm in diameter immediately before the sample. Samples were contained in 1 mm pathlength quartz cells (Type 110, Hellma) and mounted in a temperature-controlled multi-position sample changer thermostatted at 27 °C. Raw detector data were corrected and reduced to 'intensity' *vs.* Q using the Mantid framework (version 5.1)[52] and then subsequently least-squares fitted using the NIST SANS analysis package within Igor Pro.[53]

A core–shell sphere model[54,55] was used to fit polymer-only aggregates, and a core–shell bicelle model[55] used to fit nanodiscs. Schematics for these are detailed in Fig. 3(a) and (b). To fit the full Q-range, it was occasionally necessary to combine these models with a core–shell cylindrical model (Fig. 3c) to account for low concentrations of larger structures present at low-Q, using the 'sum model' function within the NIST SANS analysis package which creates a linear combination of two models. Multiple solvent contrasts were used to isolate the various structural components of each sample and were fitted simultaneously. Model parameters that were held constant during fitting, such as the solvent scattering length density (SLD) and structure factor parameters (screened Coulomb),[56] can be found in Tables S7 and S8 in the SI. Bicelle models were modified to take advantage of simultaneous fitting of multiple contrasts by allowing the percentage copolymer in the nanodisc core, and percentage hydration of the rim, to be fitted as separate variables using eqn (1) and (2)

$$\mathrm{SLD_{rim}} = (X_{\mathrm{solvent}} \times \mathrm{SLD_{solvent}}) + ((1 - X_{\mathrm{solvent}}) \times \mathrm{SLD_{polymer}}) \quad (1)$$

$$\mathrm{SLD_{core}} = (\mathrm{SLD_{lipid\ tails}} \times (1 - X_{\mathrm{polymer}})) + (X_{\mathrm{polymer}} \times \mathrm{SLD_{polymer}}) \quad (2)$$

where the mole fraction of solvent or polymer, X_{solvent} or X_{polymer}, are fitting variables. Volume percent hydration in the shell of the spherical aggregate models was calculated from the percentage difference in the fit SLD to that of the copolymer alternating block and solvent.

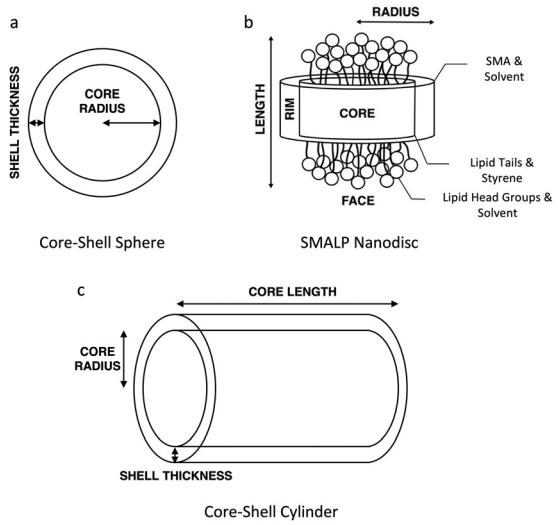

Fig. 3 (a) Cross-sectional schematic of core–shell sphere and (b) schematic of core–shell bicelle models used to fit aggregates and SMALP nanodiscs, respectively. Bicelle model comprises two ''SMALP faces'' composed of a layer of lipid head groups, 57% hydrated, and a ''SMALP core'' composed of lipid acyl chains and styrene (Full details in Table S8 in the SI). (c) Schematic of a core–shell cylinder summed with the other models to account for scattering at low-Q related to low concentrations of larger structures. Variations of schematics used in previous work.[22]

Results and discussion

Characterisation of copolymers

As in previous studies,[22,39] GPC chromatograms (Fig. 4a and Table 1), indicated that 'Fwd SMAnh' was synthesised with a lower dispersity, $Đ$, than SMA 2000Anh (1.21 *vs.* 1.89, respectively). ^{1}H and ^{13}C NMR spectroscopy confirmed the 2 : 1 Sty : MAnh ratio and the block copolymer architectures (Fig. S1 and S2, SI). Peaks were broader in the spectra for SMAnh 2000, which also lacked the peak at 36.3 ppm corresponding to alternating MSM triads present in the RAFT copolymers, instead showing additional absorption between 37–39 ppm, indicative of SSM or MSS triads[57] This was not significantly present in the spectra from the RAFT copolymers, confirming that any gradient region between the blocks was short, comprising at most a few monomer units.

A two-step reaction was employed to produce a copolymer of as similar a composition and structure to 'Fwd SMAnh' as possible, but with inverted end groups. The reaction to produce the initial polystyrene block was significantly slower than those involving styrene and maleic anhydride, so longer reaction times and higher temperatures were needed (Table S3, SI)

Optimisation of the reaction conditions to balance high conversion with formation of dead chains produced a RAFT terminated polystyrene block which, as shown in Fig. 4b, was chain extended using a mixture of styrene and maleic anhydride to yield the target 'Rev SMAnh'. Incorporation of MAnh can also be seen from FTIR spectroscopy (Fig. S3a, SI).

A similar approach produced a triblock variant, in this case a 2 : 1 Tri SMAnh with two styrene blocks each of length approximately equivalent to that in Fwd SMAnh. GPC (Fig. 4c and Table 1) and NMR (Fig. S2, SI) characterisation confirmed the target structure as described in Fig. 2b.

To increase the number of available contrasts for neutron scattering studies, partially-deuterated variants were also synthesised using deuterated styrene, aiming to create samples as similar to their hydrogenated counterparts as possible. The GPC chromatograms show that this was well achieved (Fig. 4b and Table 1), meaning chain length and structural effects between these samples should be similar.

FTIR spectroscopy (Fig. S3b, SI) showed successful hydrolysis of each of the anhydride copolymers to the corresponding

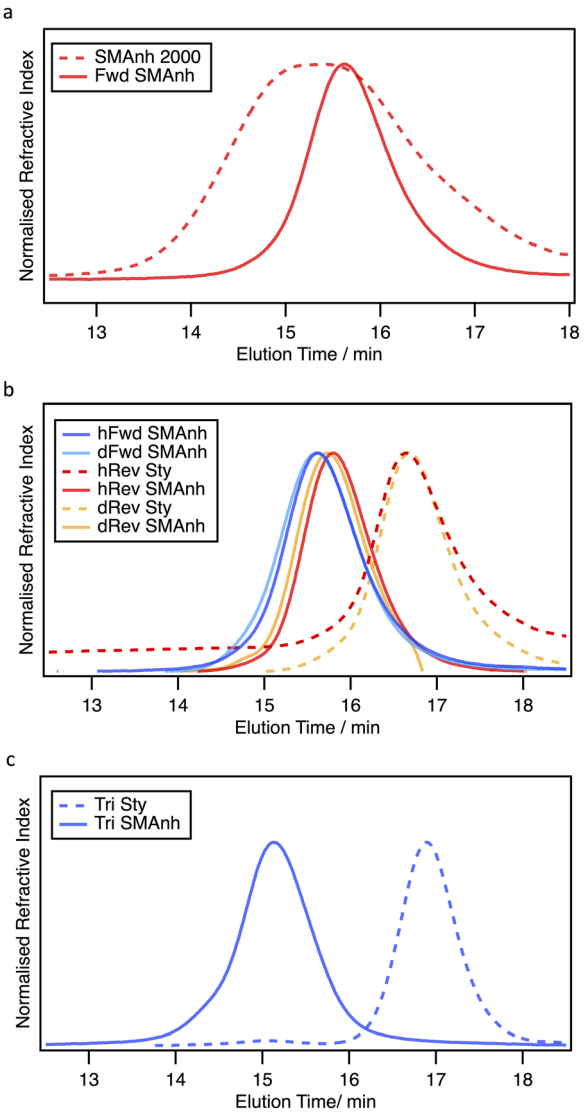

Fig. 4 GPC chromatograms for precursor polymers (before hydrolysis) in THF: (a) SMAnh 2000 and Fwd SMAnh. (b) Sty blocks and Fwd and Rev SMAnh copolymers including both hydrogenated, 'h', and deuterated, 'd', variants. (c) Tri Sty, the macro-RAFT-agent Sty block precursor for Tri SMAnh synthesis (dashed) and Tri SMAnh (solid), the copolymer resulting from triblock-type polymerisation.

acid form, SMA. The SC_{12} end groups afforded by RAFT are characteristically yellow and can be identified by the peak at 310 nm using UV/vis spectroscopy.[22,35] All copolymers retained this peak post-hydrolysis (Fig. S5, SI), indicating that the group remained intact.

Aggregation of SMA in solution

At concentrations relevant for nanodisc formation, SMA copolymers, including 1 : 1 copolymers,[58] suspended in aqueous solution have been found to exist as aggregates with a narrow size distribution.[18,59] Compared with pseudo-random copolymers such as SMA 2000, RAFT copolymers preferentially form larger, more-disperse aggregates, likely driven by the hydrophobic regions of the block architecture and co-location of hydrophobic units.[22] Previously, separate small angle X-ray (SAXS) and neutron scattering (SANS) studies[22,39] have found that aggregates from RAFT, as well as other,[16,18,58,59] SMA copolymers are structured with hydrophobic domains surrounded by hydrophilic regions, comprising one or several solvent-protected styrene cores with an acid-rich shell, ranging from spherical to ellipsoidal in shape. Prior to nanodisc formation, these aggregates must first unfold to interact with lipid bilayers.[39] Hence, exploration of the physiochemical properties of SMA in solution can give important mechanistic insights into its potential interaction with membranes. In particular, by examining the size and shape of these aggregates in response to heat, steric or thermodynamic effects associated with partitioning of the copolymer blocks may be inferred.[22,39,59]

At 25 °C, dynamic light scattering (DLS) measurements suggest that the pseudorandom SMA 2000 formed the smallest structures (2–3 nm) compared with the RAFT copolymers synthesised in this work (~13–18 nm) (Fig. 5). This was to be expected, as the RAFT copolymers have large, hydrophobic styrene blocks that need to be accommodated in the core of a self-organised aggregate. Of the RAFT copolymers, Fwd SMA produced the smallest and least disperse aggregates, whereas Rev SMA, with the opposite end-groups, formed the largest and most disperse. Interestingly, despite the longer chain length, the Tri SMA variant which has one of the two styrene blocks still conjugated to an SC_{12} group, presented a mid-way diameter and dispersity, indicating that the combination of the most hydrophobic styrene block and end group is important for minimising the size of these aggregates. Suspensions of both Rev and Tri SMA aggregates lowered the air:PBS interfacial tension slightly more than Fwd SMA (Table S5, SI), suggesting more of these species could segregate to the interface. This in turn suggests that it was slightly less favourable for these species to form solution aggregates which remove copolymer chains from the surface. All the RAFT copolymers gave much lower changes in interfacial tension values than SMA 2000.

Upon heating to 65 °C, SMA 2000 showed a significant and irreversible increase in aggregate diameter, likely representing an increase in the number of chains per particle. This may be being driven by a number of effects, likely a mixture of thermal disruption to hydrogen bonding and a decreased dielectric of the solvent at increased temperatures, reducing interaction with the solvation shell and charge repulsion, respectively. In contrast, Fwd SMA aggregates contracted slightly upon heating, a change that was reversible. We believe this could be being driven by increased mobility of the styrene block improving its ability to pack into the aggregate core at elevated temperatures (Tg(polystyrene) ~107 °C;[60] Tg(FwdSMA) ~80–90 °C from DSC in Fig. S4, SI). Heating Tri and Rev SMA suspensions appeared to permanently stabilise aggregates into smaller, less disperse structures. Here, the more pronounced effect could be indicative of a less stable starting structure. As the styrene block in these cases was terminated by mismatched, hydrophilic CN/COOH end groups, insertion into the core was unfavourable, and so heat treatment may have been needed to allow the structure to equilibrate. Again, the Tri SMA variant

Table 1 Physiochemical properties of copolymer variants, prior to hydrolysis, derived from chromatograms in Fig. 4. (Left) Macro-RAFT agent (1°-pSty). (Right) Full copolymer (SMAnh). Note that 1°-Sty denotes the first styrene block while 2°-Sty is the length of any secondary styrene block grown onto the macro-RAFT agent

Polymer	M_n/kDa[a]	$Đ$[b]	DP_n (1°-Sty)[c]	M_n/kDa[a]	$Đ$[b]	DP_n (2°-Sty)[c]	DP_n (MAnh)[c]	Length 2°-styrene block[d]	Monomer ratio[e]	Mass conversion/%
SMAnh 2000	—	—	—	3.75	1.89	—	—	—	2 : 1	—
[d]hFwd SMAnh	—	—	—	5.13	1.21	31	16	15.5	2 : 1	72.4
[d]dFwd SMAnh	—	—	—	4.96	1.20	30	15	15.0	2 : 1	64.2
[f]hRev SMAnh	1.90	1.26	15	4.64	1.13	28	14	0.0	2 : 1	65.4
[f]dRev SMAnh	1.90	1.21	15	4.72	1.12	28	14	0.0	2 : 1	69.3
Tri SMAnh	1.65	1.10	12	7.49	1.17	47	23	11.0	2 : 1	73.6

[a] Estimated from GPC chromatograms against a polystyrene standard (please see Experimental section). [b] $Đ = M_w/M_n$. [c] Degree of polymerisation $DP_n = ((M_n - M_{r(\text{end groups})}) \times \text{monomer ratio})/M_{r(\text{monomer})}$; $M_{r(\text{end groups})} = 364\ \text{gmol}^{-1}$. [d] Length styrene block in monomer units = $DP_{n(2°\text{-Sty})2} - DP_{n(1°\text{-Sty})1} - DP_{n(\text{MAnh})}$. [e] Determined from ^{1}H NMR. [f] h/d denotes hydrogenated and partially deuterated (d_8-Sty) respectively.

demonstrated behaviour intermediate between the Rev and Fwd SMA variants, adding weight to the rationale that these effects relate to the styrene block and its availability to drive aggregation.

Following previous SANS studies on Fwd SMA aggregates,[22] aggregates from Rev SMA synthesised from both hydrogenated (Rev hSMA) and deuterated styrene (Rev dSMA) were investigated by fitting SANS data at 27 °C. Contrasts of 100% and 50% D_2O PBS were used to highlight the shell and core components, respectively. Whilst the two contrasts for each sample were fitted simultaneously, the Rev hSMA and Rev dSMA samples would not fit to the same parameters when using any of the model variants described below.

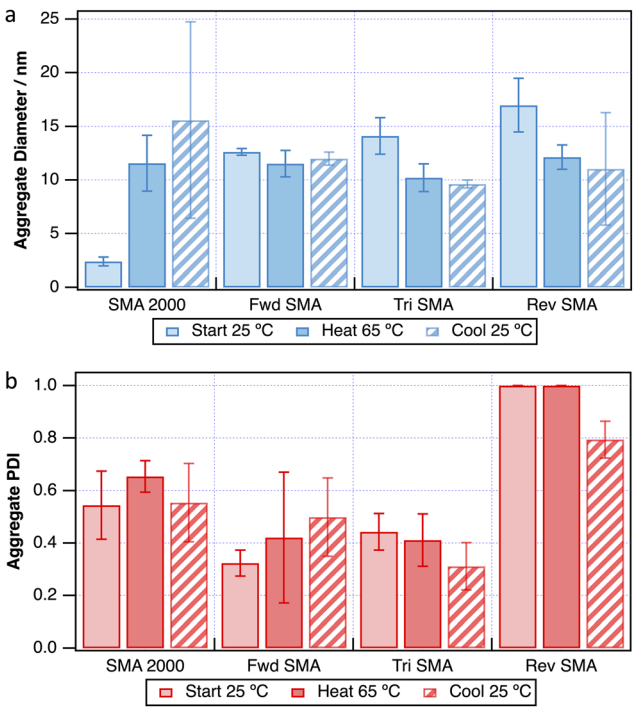

Fig. 5 DLS results from variant copolymer aggregates (1.65 wt%. in PBS), measured at 25 °C, 65 °C, and again at 25 °C: (a) mean diameter and (b) mean polydispersity. Error bars represent 95% confidence intervals.

Initially, data were fit to a spherical core–shell model (see Fig. 3a), the results of which can be found in Fig. S7a and b in the SI. Whilst this fitted the slope well at mid-Q, the model could not capture the upturns present in the low-Q region ($Q < 0.01$ Å^{-1}). This upturn is suggestive of larger scale (>100 nm), higher-order aggregation and appears to be exaggerated in the deuterated samples.[22] This could be due to differences in hydrogen bonding which may also play an important role in mediating SMA aggregate organisation. Furthermore, DLS traces of the Rev SMA showed multimodal particle size distributions compared with those for the Fwd SMA copolymer, indicating the presence of larger (~100 nm) species in solution (see Fig. S8 in the SI). Hence, by holding the spherical fits constant and summing with a core shell cylinder model (see Fig. 3c) to represent a low concentration of these larger aggregates, it was possible to successfully capture the data at mid- and low-Q (Fig. 6a and b; full parameters in Tables S9 and S10 in SI). This revealed longer, rod-like cylinders 8.5 ± 0.4 nm in radius and 53 ± 10 nm in length for h-SMA and 14 ± 10 nm in radius and 160 ± 100 nm in length for d-SMA aggregates, whereas larger-scale spheres did not fit the entire Q-range in either case. Malardier-Jugroot *et al.* previously found SMA copolymers to form nanotubes in solution,[61] and the structures seen here could reasonably represent something similar. More detailed analysis can be focused on the better defined, smaller spherical particles evident at mid-Q. The spherical Rev-SMA aggregates were found to consist of a styrene core, 3.2 ± 0.2 and 2.4 ± 0.1 nm in radius, for Rev hSMA and Rev dSMA, respectively, and a 1 : 1 Sty : MA shell with corresponding thicknesses of 0.9 ± 0.3 and 1.0 ± 0.5 nm (total diameter = 8 ± 1 nm and 7 ± 1 nm for Rev hSMA and Rev dSMA aggregates, respectively). This aligns well with the DLS results with the higher polydispersity values relating to the multimodal size distributions within the Rev SMA samples. Notably, the shell was not particularly hydrated, containing ~13 ± 8% vol. solvent. Previous studies of aggregates from Fwd SMA using SANS, found a similar shell thickness, but with a

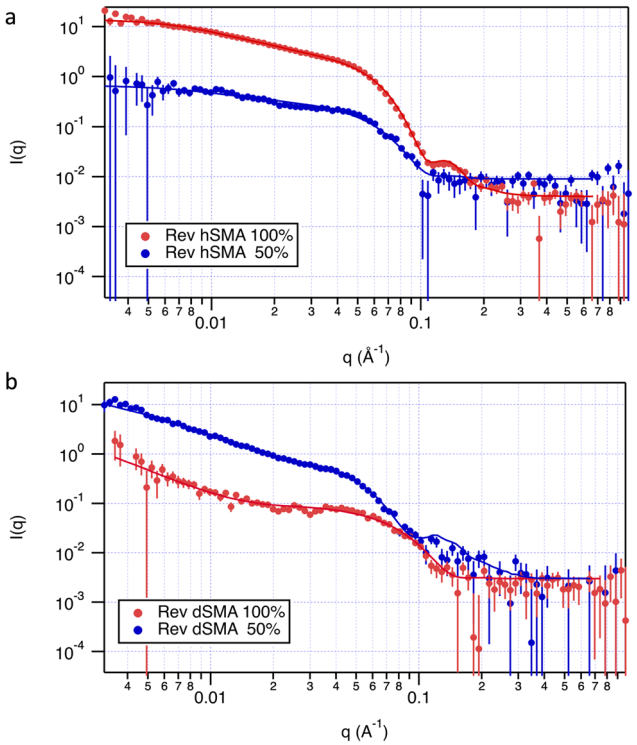

Fig. 6 SANS data from aggregate suspensions (1.65% (w/v) copolymer and 0.55% (w/v) lipid) in PBS of either 100% or 50% D_2O contrast (a) Rev hSMA; (b) Rev dSMA. Contrasts for each sample were fit simultaneously; hSMA and dSMA samples did not fit to the same parameters. Continuous lines represent fits to a summed model including both a core shell sphere model with a polydisperse radius and a low concentration of larger-scale core shell cylindrical aggregates to capture the data at low-Q. Full fitting parameters can be found in Tables S9 and S10 in the SI.

higher level of shell hydration of 40 ± 10% vol.[22] In the Rev-SMA copolymer, the alt-block is terminated by SC_{12} rather than the typical CN/COOH. Incorporating this large, hydrophobic end group into the aggregate shell might be expected to reduce shell hydration. Indeed, this was supported by the small decrease in zeta potential for Rev SMA (−17 ± 3 mV) compared to the Fwd (−24 ± 2 mV) and Tri SMA (−26 ± 1 mV) aggregates, indicating that the portion of the outer shell containing charged units was lower (Table S6, SI). Termination of the alt-block with SC_{12} might also more likely lead to bridging flocculation between copolymer micelles, thus accounting for the larger, cylindrical 'strings' of aggregates needed for the summed model. Incorporation of SC_{12} into the hydrophobic core could also be expected to lead to a larger and more spherical form compared with Fwd SMA aggregates. Previously, modification of Fwd SMA by cleaving all SC_{12} end groups to smaller, less hydrophobic CN groups ('Fwd SMA-CN') led to the aggregates adopting prolate-like cylindrical structures that could not be fitted to a sphere model.[22] When this data is compared with the current results (Fig. S7c, SI), the progressively steeper gradients at mid-Q between the Fwd SMA-CN, Fwd SMA, and Rev SMA samples, tentatively indicates reduced elongation, suggesting that Rev SMA has the most spherical structure and disrupting the usual end groups in either cases increased the larger scale aggregation seen at low-Q. This demonstrates that, not only those end groups present on the styrene block, but those on the alternating block also influence the structure and stability of the aggregates. Collection of further SANS data on the triblock as well as other block variants of RAFT-made SMA will facilitate further investigation of this

Formation and structure of lipid-copolymer nanodiscs

Although several means of quantifying nanodisc formation have been explored including fluorescence techniques[29,62] and surface pressure isotherms,[38] one of the most easily applied is turbidimetry.[58] UV-visible absorbance is measured as a function of time and the rate of formation of nanodiscs is related to the rate of fall in light scattering as the solution clarifies when lipids are removed from large (>100 nm) multilamellar vesicles to form the smaller structures.

As will be seen in the following section, nanodiscs with typical size and shape were present in solution after 24 h incubation of DMPC lipid suspensions with each of the four copolymers studied here. However, there were significant differences in the behaviour of each system immediately after mixing. For example, measurement of turbidity changes at 37 °C are shown in Fig. 7a. After injection of the copolymers, a small initial rise in scattering occurs, presumably due to mixing and stirring effects, after which a fall of absorbance is measured.

Addition of SMA 2000 to a suspension of DMPC rapidly clarified the suspension indicating the incorporation of the majority of lipids into nanodiscs over a very short timescale of ~20 s (Fig. 7a). The process was much slower when the RAFT-synthesised copolymers were used. For example, Fwd SMA instead clarified the solution over a timeframe of around 25 min. Rev SMA appeared to be unreactive over this timescale so that nanodisc formation was very much slower in comparison. Once again, the triblock copolymer demonstrated intermediate behaviour. There was only a very small initial change in absorbance but further reaction occurred after around 15–20 min.

To allow further comparison, the fall in the initial rate of absorbance immediately after mixing at 37 °C was measured (see Fig. S6a, SI). As described in Section 2.4 of the SI, the values of rate derived from the above results were: −(0.410 ± 0.040) s^{-1} for SMA 2000, −(0.022 ± 0.005) s^{-1} for Fwd SMA, −(0.004 ± 0.001) s^{-1} for Rev SMA and –(0.011 ± 0.005) s^{-1} for Tri SMA (negative rates of change of absorbance correspond with rates of formation of nanodiscs), confirming that the arrangement of groups along the chain and their different morphologies influences the initial interactions between the copolymers and the lipids. To exclude any chain length dependence, further comparison of SMA 2000 with Fwd SMA of different molar masses was conducted at three additional temperatures, 15 °C, 20 °C and 25 °C (Fig. S6b and c, SI). As might be expected, the rate of nanodisc formation increased with temperature but the process with SMA 2000 always proceeded at a significantly faster rate than Fwd SMA. Fig. 7b shows these rates and demonstrates that the effect of changing molar mass was small in comparison with

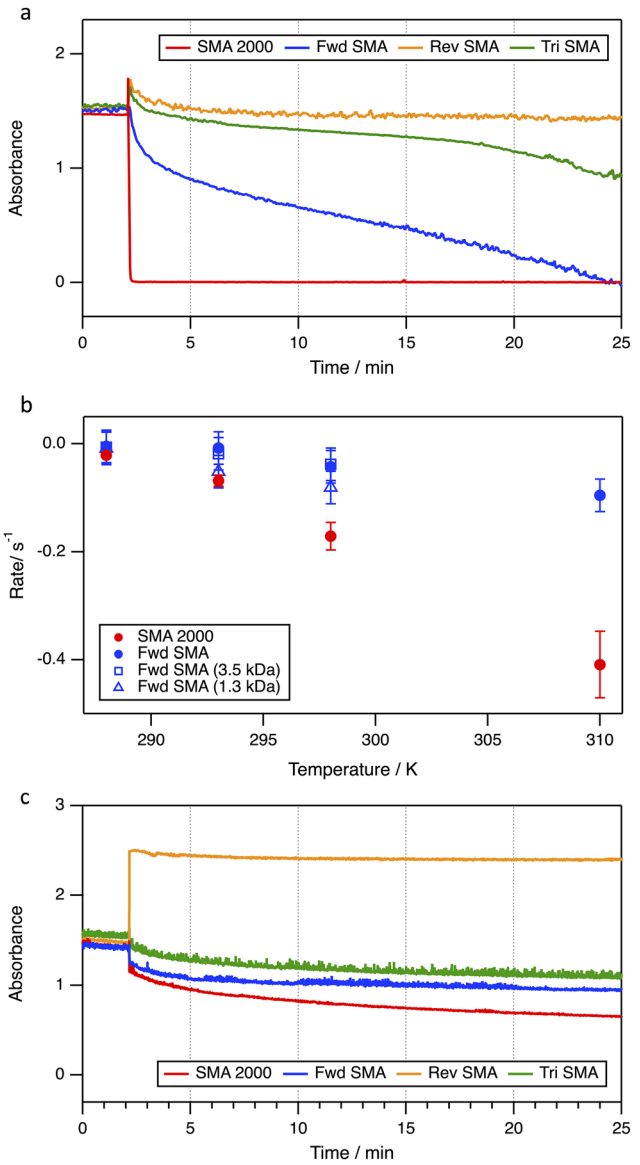

Fig. 7 (a) UV-vis absorbance due to scattering at 450 nm on adding SMA to DMPC vesicle suspensions at 37 °C. (b) Initial rate of change of absorbance for SMA 2000 and Fwd SMA of varying chain lengths (c) as (a) on adding SMA to *E. coli* membrane suspensions at 37 °C.

the differences from SMA 2000. In particular, it would be expected that shorter chains would interact faster and more effectively due to faster diffusion, although here this was not significant. It is apparent that changes in chain length do not account for the differences in rates between the two series of copolymers. This confirmed that variations in the chain length can be discounted when comparing Fwd, Rev and Tri-SMA copolymers.

All of the RAFT structures were much slower to form nanodiscs than SMA 2000. It has been suggested that nanodisc formation proceeds *via* an insertion–disruption mechanism.[18,19,26] The results here are consistent with this suggestion and can be explained in terms of the balance of hydrophilicity and hydrophobicity of the copolymer blocks and end groups. The Rev SMA copolymer, with mis-matched end group properties, had the longest delay to solubilisation, suggesting that the end groups may interfere with the hydrophilicity of the alternating block and styrene block, impacting their role in nanodisc formation. As was the case with aggregates, the Tri SMA copolymer presented intermediate properties, for example the latency time was similar to that of Fwd SMA, but there was slight agglomeration upon introduction to DMPC, as with Rev SMA.

Simple measurements of the initial rate of change of absorbance did not give a full description of nanodisc formation. For example, the Tri and Rev SMA variants appeared to agglomerate slightly during the initial period (Fig. 7a). Moreover, even after 25 min, the Rev variant did not solubilise DMPC. However, given sufficient time, nanodiscs do form as shown by the light scattering results below. There have been a number of reports suggesting that some RAFT copolymers do not form nanodiscs but it may be that their formation was limited by these kinetic effects and, in some circumstances, it can be beneficial to monitor changes in properties over a much longer timescale, particularly when comparing the behaviour of RAFT copolymers.

The ability to form nanodiscs here can be influenced by the composition and structure of the target membrane.[36,63] The ultimate aim of using such copolymers is the extraction of membrane proteins and their lipids from cell membranes. It has been documented that forming nanodiscs with Gram negative *E. coli* membranes is much slower and proceeds to a lesser extent with RAFT copolymers.[35,48] Experiments here using mixed inner and outer *E. coli* membrane suspensions showed that although SMA 2000 could quickly solubilise a reasonable amount of membrane (Fig. 7c), addition of RAFT copolymers induced only a very slow reduction in absorbance. However, solubilisation for all copolymers continued for more than 24 h. Again, the Tri SMA variant presented similar, but slightly slower, solubilisation behaviour compared to Fwd SMA.

Rev SMA, the only variant not to contain an SC_{12}-terminated styrene block, appeared to aggregate the *E. coli* membrane. *E. coli* bacteria contain protective lipopolyscharides on the surface and this layer would normally reduce transport of hydrophobic solutes across the outer membrane.[64] Here, the hydrophobic SC_{12} end group terminating the alt-block may have caused bridging aggregation between hydrophobic regions, possibly between the lipopolyscharides. Alternatively, the alternating blocks, unable to penetrate the bilayer, may have undergone self-aggregation to minimise solvent interaction. Regardless, if this effect can be exacerbated by inversion or modification of the copolymer end groups alone, a powerful means to modulate and tailor RAFT copolymers towards target membranes could lie with variants in end group chemistry.

Polydisperse SMA samples, such as SMA 2000 which also have pseudorandom copolymer architectures, are consistently found to produce the smallest and most monodisperse nanodiscs with both native and model membranes. It is thought that the diverse range of properties arising from a broad distribution of copolymers, as well as co-operative effects between chains of different length, can act to minimise interfacial forces.[13,34,65] RAFT-synthesised SMA copolymers, having more

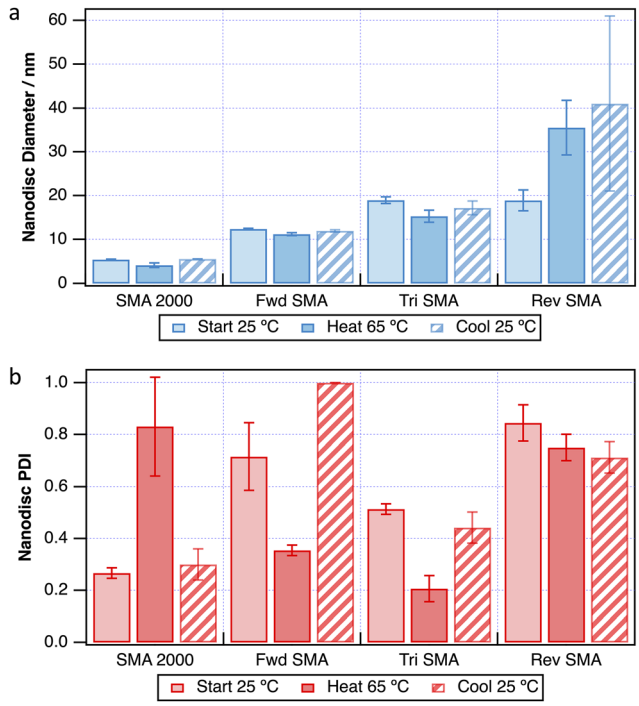

Fig. 8 DLS results from nanodiscs formed from DMPC lipids and SMA copolymers in PBS (1.65% (w/v) copolymer and 0.55% (w/v) lipid) incubated for 24 h then measured at 25 °C, 65 °C, and again at 25 °C. (a) Mean nanodisc diameter and (b) mean nanodisc polydispersity Error bars represent 95% confidence intervals.

segregated hydrophobic and hydrophilic domains, typically produce larger and more polydisperse nanodiscs.[48] DLS measurements at 25 °C on the nanodiscs formed on copolymers produced here (Fig. 8) followed this pattern. SMA 2000 yielded nanodiscs approximately 5 nm in diameter with a polydispersity of 0.3. As expected, the RAFT copolymers all formed nanodiscs larger and more polydisperse than this. The Fwd SMA variant produced the smallest of the three, approximately 12 nm in diameter, followed by the Tri and then Rev SMA samples, each approximately 19 nm in diameter.

When these nanodisc mixtures were heated to 65 °C, a small, reversible contraction in radius was seen for all except the Rev-SMA containing nanodiscs. For commercial copolymers such as SMA 2000, this has been reported previously,[66] particularly around the Tg of DMPC (~ 24 °C). For the RAFT copolymers, this contraction was accompanied by a decrease in polydispersity and could represent restructuring of the styrene blocks that were kinetically trapped at lower temperatures either due to the increased mobility of the styrene block or increased mixing of the styrene and aliphatic chains at higher temperatures. The exception in behaviour was seen for Rev SMA, where heating induced irreversible macro-aggregation (>40 nm diameter). In this case, the presence of the SC_{12} end group on the alternating block may cause bridging between aggregates, as this group, attached to the hydrophilic part of the polymer may be able to anchor itself easily into neighbouring lipid bilayer structures. Capping the styrene block by a hydrophilic group may also contribute to this by inhibiting its efficient penetration into the disc core.

Recently published data provides further support for these suggested effects. RAFT SMA with styrene : MAnh ratios of 2 : 1–3.1 have been produced[73] using a photoinitiation technique which yield copolymer structures similar to those of the commercial materials with low dispersity but without a polystyrene block. This showed similar protein solubilization efficiency to the commercial SMA copolymers. Also, Gomes *et al.*[74] recently produced RAFT SMA copolymers capped with hydrophilic poly(ethylene glycol) moieties. Interestingly, they demonstrated that for the 1 : 1 copolymer (presumably lacking a polystyrene block), the length of the PEG had no significant effect on the solubilization of DMPC membranes. However, copolymers with higher styrene contents (SMA(2 : 1) and SMA(3 : 1)) showed distinctly different behaviour between short and longer PEG lengths. Clearly, there is a very subtle interplay between the hydrophobicity along the chain and particularly in blocks and the end groups.

SANS data of nanodisc suspensions from both Rev h-SMA and d-SMA could not be fitted using only the core–shell bicelle model (Fig. 3b), in contrast to those from Fwd SMA.[22] The best fit achieved with this model was unable to capture the steep gradient present at mid-*Q* (Fig. S9 and Table S13, SI), signifying that this form had a larger aspect ratio than the model described. Moreover, the model for this fit gave an unreasonabe dispersity (0.25), especially compared with results from DLS.

Typically during fitting, the length of the nanodisc was held constant at 2.8 nm to be consistent with a DMPC bilayer.[15,67] While releasing this parameter increased the disc length to 5.3 ± 0.3 nm (Fig. S10 and Table S14, SI), and somewhat improved the fit, the model remained unable to capture prominent features in the data. Although this was found to be an unsatisfactory fit overall, it is interesting that the disc length roughly doubled. Others have identified face-to-face or 'rouleaux' stacking of commercial SMA[68] and RAFT SMA nanodiscs,[35] as well as membrane scaffold proteins[69,70] and amphiphile nanodiscs,[71] through negative stain transmission electron microscopy (TEM). In this regard, a model representing a stack of two nanodiscs was attempted (Fig. S11 and Table S15 in SI) using the 'stacked disc' model, representing two face-to-face stacked fragments of lipid bilayers. This was able to capture more of the features at mid-Q, notably for the 35% D_2O PBS solvent contrast, which matches the hydrogenated copolymer annulus not accounted for in this model. However, features in the other contrasts such as the 50% D_2O PBS could not be recreated. A stack of 50 fragments, whilst capturing more of the data at low-Q, remained a poor fit overall (Fig. S12 and Tables S16, S17 in the SI). We have noted some minor deviation from these bicelle models elsewhere. For example, *ab intio* models without deterministic form factors, found polymer located outside the annulus and discs with slightly ellipsoidal radii.[20] We have also previously fitted SAXS data by describing a mixed suspension, combining nanodisc models with models representing the corresponding copolymer aggregates.[39]

Here, a combined core shell bicelle + core shell sphere model was found to best fit the data for both Rev hSMA and

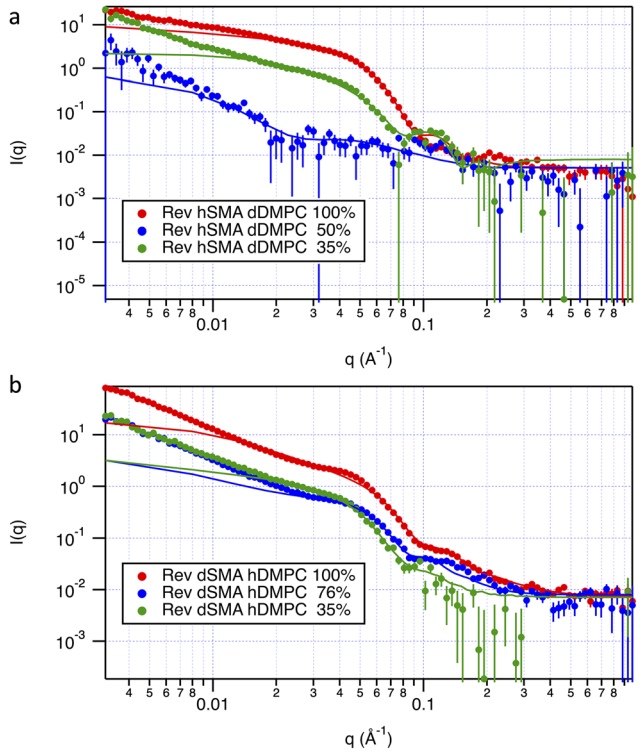

Fig. 9 SANS data from (a) Rev hSMA and dDMPC and (b) Rev dSMA and hDMPC SMALP nanodisc suspensions in PBS (1.65% (w/v) copolymer and 0.55% (w/v) lipid) of various contrasts. Continuous lines represent fits to a combined core shell bicelle + core shell sphere model. Full fitting parameters can be found in the SI.

dSMA nanodiscs, across the entire Q range (Fig. 9; Full fitting parameters can be found in Tables S11 and S12, SI). Aggregate parameters used here, including polydispersity and hydration, were largely in line with those found for the copolymer-only samples (Tables S9 and S10, SI). Nanodisc polydispersities (0.60 ± 0.05) were also now more aligned to results from DLS and previous SANS findings. Likewise, freely-fitted nanodisc lengths returned to the anticipated 2.8 ± 0.2 nm. This was accompanied by an approximately 10% decrease in hydration of the nanodisc rim compared to Fwd SMA;[22] a reasonable difference given that the hydrophilic alternating block has been capped by an SC_{12} group. Similarly, approximately 10% lower volume of the nanodisc core was occupied by polymer than in the Fwd SMA nanodiscs,[22] indicating reduced ability of the styrene block to penetrate the lipid tails due to capping with a hydrophilic group. Disruption to lipid tail packing is known to be crucial for nanodisc formation[13,19,72] and these results add weight to the theory that the styrene block plays a large part in driving the process. Again, this model failed to capture the upturn in gradient seen at $Q < 0.01$ Å^{-1}, indicative of larger-scale aggregation. It was possible to fit the data at low-Q by summing the bicelle model with the large cylindrical structures found in the aggregate solutions (Fig. S13; full fitting parameters in Tables S18 and S19 in the SI), possibly representing copolymer or copolymer aggregates unable to dissociate and interact with lipids.

A comparison of all models used to fit the Rev hSMA dDMPC nanodisc data can be found in Figure S14 in the SI. In reality, the samples will likely contain a mixture of SMALP nanodiscs, nanodisc stacks, smaller (<10 nm) spherical aggregates, and larger-scale (>100 nm) higher-order aggregates arising from bridging flocculation caused by capping the hydrophilic alt-block with a hydrophobic SC_{12} group. Irrespective of the exact morphological identity, data from SANS and DLS clearly demonstrate that reversing the end groups has led to significant aggregation external to the nanodiscs, either with the copolymer itself, membrane, free lipid or a combination of these. As end group inversion has directly impacted the efficacy of the copolymer to solubilise membranes in comparison to other copolymers synthesised by RAFT, it stands that the alternative must also be true. By optimising end group chemistries to work desirably in conjunction with corresponding block architectures, more efficient nanodisc behaviours may well result, enhancing and expanding the range of possible applications.

Conclusions

RAFT SMA copolymer variants were successfully synthesised with equivalent M_w but inverted block architecture and chain end groups. SMA as typically synthesised has an alternating styrene-maleic acid block terminated by a hydrophilic CN or COOH end group, connected to a styrene block terminated by a hydrophobic SC_{12} end group. By employing a two-step RAFT polymerisation, we have prepared a variant comprising a styrene block terminated by CN or COOH attached to an alternating block with a SC_{12} end group. The balance of hydrophilicity and hydrophobicity is thus changed. These copolymers were further compared to a RAFT-synthesised triblock material containing both a SC_{12} and a CN/COOH terminated styrene block, as well as a commercial SMA 2000 variant which has a broad distribution of M_w and pseudo-random monomer sequence.

All the copolymers were found to form higher-order aggregates in aqueous PBS solution. SANS measurements showed that the RAFT copolymer aggregates were structured as spheres comprising a styrene core and acid-rich shell. Upon heating to 65 °C, an irreversible decrease in diameter was seen for those RAFT copolymers containing a styrene block adjacent to a CN or COOH group. Rev SMA, containing a SC_{12} terminated alternating block, was found to form more spherical, than ellipsoidal, particles, attributed to the increased size of headgroup to be accommodated in the copolymer micelle. Copolymers were also found to form larger scale (>100 nm), rod-like cylindrical aggregates compared to Fwd SMA, likely due to bridging flocculation arising from capping the hydrophilic alt-block with a hydrophobic SC_{12} group. Complimentary imaging techniques, such as TEM or fluorescence imaging, could be beneficial in further study.

In contrast to SMA 2000, which formed small, monodisperse nanodiscs very quickly with model lipids, removal of lipids by the RAFT copolymers was slower which is related to the insertion mechanism. The relative rates can be correlated with the

hydrophobic balance of the end groups. Rev SMA was found to form the largest, most polydisperse nanodiscs, slowest. Investigation into polymer:lipid ratios used for formation might provide important clues on the interactions responsible. Moreover, the availability of deuterated pseudo-random copolymers would facilitate study of the commercial variants currently used by the majority of researchers. Regardless, for RAFT copolymers, it seemed that a styrene block capped by a hydrophobic group plays a critical role in effective membrane solubilisation.

The study highlights not only how the overall amphiphilic balance of the copolymer is important, but how the distinct distribution within the chain, down to the sequence of copolymer blocks and respective end groups, are significant considerations towards controlling their solution structures as well as their interactions with lipids and hence nanodisc formation. Large differences in behaviour were observed with copolymers of near equivalent composition and molar mass but inversion of block structures and end groups. A deeper appreciation of these dynamics will enable not only the intentional adjustment of copolymer end group chemistries to facilitate favourable interactions with difficult-to-target MPs, but the potential to functionalise the copolymer through these end groups, thereby expanding the scope of possible applications for nanodiscs.

Author contributions

The manuscript was written through contributions of all authors. GMN: conceptualisation, methodology, investigation, visualisation, writing – original draft, writing – review & editing; AAN: investigation, writing – review & editing; JD: SANS investigation, writing – review & editing; SK: SANS investigation, writing – review & editing; PE: conceptualisation, supervision, writing – review & editing; PW: conceptualisation, methodology, supervision, writing – review & editing; GJP: conceptualisation, methodology, supervision, writing – review & editing; KJE: conceptualisation, methodology, supervision, funding acquisition, writing – review & editing.

Conflicts of interest

There are no conflicts to declare.

Data availability

Data supporting the results in this paper are available through the University of Bath Research Data Archive: https://doi.org/10.15125/BATH-01635.

Supplementary information: polymer synthesis and characterisation, solution behaviour, rates of nanodisc formation and SANS data and fitting parameters. See DOI: https://doi.org/10.1039/d5sm01014d.

Acknowledgements

GMN thanks the EPSRC Centre for Doctoral Training in Sustainable Chemical Technologies (EPSRC grant EP/L016354/1) at the University of Bath for funding his PhD studies. We thank the Science & Technology Facilities Council and ISIS Neutron and Muon Source for provision of beamtime on SANS2D under beamtime allocation RB2010215. Raw data (DOI: https://doi.org/10.5286/ISIS.E.RB2010215) collected on SANS2D can be found in the ISIS-ICAT system at https://data.isis.stfc.ac.uk/doi/INVESTIGATION/111242883/. Special thanks is given to JD and SK for running the SANS experiments during lockdown. We would also like to thank Dr Rémi Castaing and Dr John Lowe at the Materials Characterisation Facility (MC^2, University of Bath) for assistance as part of their respective roles as GPC and NMR instrument specialists.

Notes and references

1 E. Wallin and G. von Heijne, *Protein Sci.*, 1998, **7**, 1029–1038.
2 O. M. Becker, Y. Marantz, S. Shacham, B. Inbal, A. Heifetz, O. Kalid, S. Bar-Haim, D. Warshaviak, M. Fichman and S. Noiman, *Proc. Natl. Acad. Sci. U. S. A.*, 2004, **101**, 11304–11309.
3 H. Ryu, A. Fuwad, S. Yoon, H. Jang, J. C. Lee, S. M. Kim and T. J. Jeon, *Int. J. Mol. Sci.*, 2019, **20**, 1437.
4 J. M. Dörr, S. Scheidelaar, M. C. Koorengevel, J. J. Dominguez, M. Schäfer, C. A. van Walree and J. A. Killian, *Eur. Biophys. J.*, 2016, **45**, 3–21.
5 G. G. Privé, *Methods*, 2007, **41**, 388–397.
6 H. E. Autzen, D. Julius and Y. Cheng, *Curr. Opin. Struct. Biol.*, 2019, **58**, 259–268.
7 RCSB Protein Data Bank, https://www.rcsb.org.
8 M. Lee, H. Yang, D. Kim, M. Yang, T. H. Park and S. Hong, *Sci. Rep.*, 2018, **8**, 13945.
9 D. Charvolin, J.-B. Perez, F. Rouvière, F. Giusti, P. Bazzacco, A. Abdine, F. Rappaport, K. L. Martinez and J.-L. Popot, *Proc. Natl. Acad. Sci. U. S. A.*, 2009, **106**, 405–410.
10 M. Zoonens and J. L. Popot, *J. Membr. Biol.*, 2014, **247**, 759–796.
11 T. H. Bayburt, Y. V. Grinkova and S. G. Sligar, *Nano Lett.*, 2002, **2**, 853–856.
12 N. G. Brady, S. Qian, J. Nguyen, H. M. O'Neill and B. D. Bruce, *Biochim. Biophys. Acta, Bioenerg.*, 2022, **1863**, 148596.
13 M. Xue, L. Cheng, I. Faustino, W. Guo and S. J. Marrink, *Biophys. J.*, 2018, **115**, 494–502.
14 Z. Stroud, S. C. L. Hall and T. R. Dafforn, *Methods*, 2018, **147**, 106–117.
15 M. Jamshad, V. Grimard, I. Idini, T. J. Knowles, M. R. Dowle, N. Schofield, P. Sridhar, Y. Lin, R. Finka, M. Wheatley, O. R. T. Thomas, R. E. Palmer, M. Overduin, C. Govaerts, J.-M. Ruysschaert, K. J. Edler and T. R. Dafforn, *Nano Res.*, 2015, **8**, 774–789.
16 V. A. Bjørnestad, M. Orwick-Rydmark and R. Lund, *Langmuir*, 2021, **37**, 6178–6188.
17 S. Scheidelaar, M. C. Koorengevel, J. D. Pardo, J. D. Meeldijk, E. Breukink and J. A. Killian, *Biophys. J.*, 2015, **108**, 279–290.

18 P. S. Orekhov, M. E. Bozdaganyan, N. Voskoboynikova, A. Y. Mulkidjanian, H.-J. Steinhoff and K. V. Shaitan, *Langmuir*, 2019, **35**, 3748–3758.
19 M. Orwick Rydmark, M. K. Christensen, E. S. Köksal, I. Kantarci, K. Kustanovich, V. Yantchev, A. Jesorka and I. Gözen, *Soft Matter*, 2019, **15**, 7934–7944.
20 K. A. Morrison, A. Doekhie, G. M. Neville, G. J. Price, P. Whitley, J. Doutch and K. J. Edler, *BBA Adv.*, 2022, **2**, 100033.
21 C. Jeong, R. Franklin, K. J. Edler, K. Vanommeslaeghe, S. Krueger and J. E. Curtis, *J. Phys. Chem. B*, 2022, **126**, 1034–1044.
22 G. M. Neville, K. A. Morrison, E. Shilliday, J. Doutch, R. M. Dalgliesh, G. J. Price and K. J. Edler, *Soft Matter*, 2023, **19**, 8507–8518.
23 T. J. Knowles, R. Finka, C. Smith, Y.-P. Lin, T. Dafforn and M. Overduin, *J. Am. Chem. Soc.*, 2009, **131**, 7484–7485.
24 SMALP.net, https://www.smalp.net/polymers.html, Accessed 15/08/23.
25 L. Eggenreich, C. Vargas, C. Kolar and S. Keller, *Biol. Chem.*, 2023, **404**, 703–713.
26 S. C. L. Hall, C. Tognoloni, R. A. Campbell, J. Richens, P. O'Shea, A. E. Terry, G. J. Price, T. R. Dafforn, K. J. Edler and T. Arnold, *J. Colloid Interface Sci.*, 2022, **625**, 220–236.
27 G. Hazell, T. Arnold, R. D. Barker, L. A. Clifton, N.-J. Steinke, C. Tognoloni and K. J. Edler, *Langmuir*, 2016, **32**, 11845–11853.
28 R. Cuevas Arenas, B. Danielczak, A. Martel, L. Porcar, C. Breyton, C. Ebel and S. Keller, *Sci. Rep.*, 2017, **7**, 45875.
29 A. Grethen, D. Glueck and S. Keller, *J. Membr. Biol.*, 2018, **251**, 443–451.
30 S. C. L. Hall, L. A. Clifton, C. Tognoloni, K. A. Morrison, T. J. Knowles, C. J. Kinane, T. R. Dafforn, K. J. Edler and T. Arnold, *J. Colloid Interface Sci.*, 2020, **574**, 272–284.
31 B. Danielczak and S. Keller, *Methods*, 2020, **180**, 27–34.
32 A. Grethen, A. O. Oluwole, B. Danielczak, C. Vargas and S. Keller, *Sci. Rep.*, 2017, **7**, 11517.
33 K. A. Morrison, L. Wood, K. J. Edler, J. Doutch, G. J. Price, F. Koumanov and P. Whitley, *Sci. Rep.*, 2022, **12**, 3532.
34 E. Kamilar, J. Bariwal, W. Zheng, H. Ma and H. Liang, *Biomacromolecules*, 2023, **24**, 1819–1838.
35 A. H. Kopf, O. Lijding, B. O. W. Elenbaas, M. C. Koorengevel, J. M. Dobruchowska, C. A. van Walree and J. A. Killian, *Biomacromolecules*, 2022, **23**, 743–759.
36 D. J. K. Swainsbury, S. Scheidelaar, N. Foster, R. van Grondelle, J. A. Killian and M. R. Jones, *Biochim. Biophys. Acta, Biomembr.*, 2017, **1859**, 2133–2143.
37 K. A. Morrison, K. J. Heesom, K. J. Edler, J. Doutch, G. J. Price, F. Koumanov and P. Whitley, *Front. Mol. Biosci.*, 2021, 8.
38 R. D. Cunningham, A. H. Kopf, B. O. W. Elenbaas, B. B. P. Staal, R. Pfukwa, J. A. Killian and B. Klumperman, *Biomacromolecules*, 2020, **21**, 3287–3300.
39 G. M. Neville, K. J. Edler and G. J. Price, *Nanoscale*, 2022, **14**, 5689–5693.
40 K. M. Burridge, B. D. Harding, I. D. Sahu, M. M. Kearns, R. B. Stowe, M. T. Dolan, R. E. Edelmann, C. Dabney-Smith, R. C. Page, D. Konkolewicz and G. A. Lorigan, *Biomacromolecules*, 2020, **21**, 1274–1284.
41 S. C. L. Hall, C. Tognoloni, J. Charlton, É. C. Bragginton, A. J. Rothnie, P. Sridhar, M. Wheatley, T. J. Knowles, T. Arnold, K. J. Edler and T. R. Dafforn, *Nanoscale*, 2018, **10**, 10609–10619.
42 T. Ravula, S. K. Ramadugu, G. Di Mauro and A. Ramamoorthy, *Angew. Chem.*, 2017, **129**, 11624–11628.
43 M. Timcenko, A. A. A. Autzen and H. E. Autzen, *ACS Appl. Polym. Mater.*, 2022, **4**, 1071–1083.
44 R. Guo, J. Sumner and S. Qian, *ACS Appl. Bio Mater.*, 2021, **4**, 4760–4768.
45 A. H. Kopf, J. M. Dörr, M. C. Koorengevel, F. Antoniciello, H. Jahn and J. A. Killian, *Biochim. Biophys. Acta, Biomembr.*, 2020, **1862**, 183125.
46 A. F. Craig, E. E. Clark, I. D. Sahu, R. Zhang, N. D. Frantz, M. S. Al-Abdul-Wahid, C. Dabney-Smith, D. Konkolewicz and G. A. Lorigan, *Biochim. Biophys. Acta*, 2016, **1858**, 2931–2939.
47 A. A. A. Smith, H. E. Autzen, T. Laursen, V. Wu, M. Yen, A. Hall, S. D. Hansen, Y. Cheng and T. Xu, *Biomacromolecules*, 2017, **18**, 3706–3713.
48 S. C. L. Hall, C. Tognoloni, G. J. Price, B. Klumperman, K. J. Edler, T. R. Dafforn and T. Arnold, *Biomacromolecules*, 2018, **19**, 761–772.
49 D. J. Keddie, *Chem. Soc. Rev.*, 2014, **43**, 496–505.
50 S. Tongue, WO 2006/129127 A1, 2006.
51 S. Harrisson and K. L. Wooley, *Chem. Commun.*, 2005, 3259–3261.
52 O. Arnold, J. C. Bilheux, J. M. Borreguero, A. Buts, S. I. Campbell, L. Chapon, M. Doucet, N. Draper, R. Ferraz Leal, M. A. Gigg, V. E. Lynch, A. Markvardsen, D. J. Mikkelson, R. L. Mikkelson, R. Miller, K. Palmen, P. Parker, G. Passos, T. G. Perring, P. F. Peterson, S. Ren, M. A. Reuter, A. T. Savici, J. W. Taylor, R. J. Taylor, R. Tolchenov, W. Zhou and J. Zikovsky, *Nucl. Instrum. Methods Phys. Res., Sect. A*, 2014, **764**, 156–166.
53 S. R. Kline, *J. Appl. Crystallogr.*, 2006, **39**, 895–900.
54 P. Bartlett and R. H. Ottewill, *J. Chem. Phys.*, 1992, **96**, 3306–3318.
55 A. Guinier and G. Fournet, *Small-Angle Scattering of X-Rays*, Wiley, New York, 1st edn, 1955.
56 J. B. Hayter and J. Penfold, *Mol. Phys.*, 1981, **42**, 109–118.
57 P. F. Barron, D. J. T. Hill, J. H. O'Donnell and P. W. O'Sullivan, *Macromolecules*, 1984, **17**, 1967–1972.
58 S. Scheidelaar, M. C. Koorengevel, C. A. van Walree, J. Dominguez, J. M. Dörr and J. A. Killian, *Biophys. J.*, 2016, **111**, 1974–1986.
59 N. G. Brady, S. Qian and B. D. Bruce, *Eur. Polym. J.*, 2019, **111**, 178–184.
60 J. Rieger, *J. Therm. Anal.*, 1996, **46**, 965–972.
61 C. Malardier-Jugroot, T. G. M. van de Ven and M. A. Whitehead, *Mol. Simul.*, 2005, **31**, 173–178.
62 G. M. Di Mauro, C. La Rosa, M. Condorelli and A. Ramamoorthy, *Langmuir*, 2021, **37**, 3113–3121.

63 J. M. Dörr, M. H. van Coevorden-Hameete, C. C. Hoogenraad and J. A. Killian, *Biochim. Biophys. Acta, Biomembr.*, 2017, **1859**, 2155–2160.
64 M. C. Wiener and P. S. Horanyi, *Proc. Natl. Acad. Sci. U. S. A.*, 2011, **108**, 10929–10930.
65 V. Schmidt and J. N. Sturgis, *Biochim. Biophys. Acta, Biomembr.*, 2018, **1860**, 777–783.
66 R. Maier, R. Cuevas Arenas, F. Zhang, A. García-Sáez and F. Schreiber, *Langmuir*, 2023, **39**, 2450–2459.
67 M. B. Smith, D. J. McGillivray, J. Genzer, M. Losche and P. K. Kilpatrick, *Soft Matter*, 2010, **6**, 862–865.
68 J. J. Dominguez Pardo, J. M. Dörr, M. F. Renne, T. Ould-Braham, M. C. Koorengevel, M. J. van Steenbergen and J. A. Killian, *Chem. Phys. Lipids*, 2017, **208**, 58–64.
69 K. Grushin, M. A. White and S. Stoilova-McPhie, *Nanotechnol. Rev.*, 2017, **6**, 139–148.
70 P. A. Beales, N. Geerts, K. K. Inampudi, H. Shigematsu, C. J. Wilson and T. K. Vanderlick, *J. Am. Chem. Soc.*, 2013, **135**, 3335–3338.
71 F. Mahler, A. Meister, C. Vargas, G. Durand and S. Keller, *Small*, 2021, **17**, 2103603.
72 L. M. Real Hernandez and I. Levental, *Biophys. J.*, 2023, **122**, 2256–2266.
73 V. Monjal, P. Guillet, A. Moreno, M. Soulié and G. Durand, *J. Polym. Sci.*, 2024, **62**, 5277–5288.
74 M. A. G. B. Gomes, D. Glueck, V. Monjal, M. Damian, P. Guillet, J.-L. Baneres, S. Keller and G. Durand, *ACS Appl. Polym. Mater.*, 2025, **7**, 14766–14780.

